Biogeosciences Discuss., 9, 15787–15821, 2012
www.biogeosciences-discuss.net/9/15787/2012/
doi:10.5194/bgd-9-15787-2012

Biogeosciences Discussions

Kinetic bottlenecks to chemical exchange rates for deep-sea animals II: Carbon dioxide

A. F. Hofmann[1,2], **E. T. Peltzer**[1], **and P. G. Brewer**[1]

[1]Monterey Bay Aquarium Research Institute (MBARI), 7700 Sandholdt Road, Moss Landing, CA 95039–9644, USA
[2]current address: German Aerospace Center (DLR), Institute of Technical Thermodynamics, Pfaffenwaldring 38–40, 70569 Stuttgart, Germany

Received: 4 October 2012 – Accepted: 28 October 2012 – Published: 9 November 2012

Correspondence to: A. F. Hofmann (ahofmann.mbari@gmail.com)

Published by Copernicus Publications on behalf of the European Geosciences Union.

Abstract

Increased ocean acidification from fossil fuel CO_2 invasion, from temperature-driven changes in respiration, and from possible leakage from sub-seabed geologic CO_2 disposal has aroused concern over the impacts of elevated CO_2 concentrations on marine life. Discussion of these impacts has so far focused only on changes in the oceanic bulk fluid properties (ΔpH, $\Delta[\sum CO_2]$ etc.) as the critical variable and with a major focus on carbonate shell dissolution. Here we describe the rate problem for animals that must export CO_2 at about the same rate at which O_2 is consumed. We analyze the basic properties controlling CO_2 export within the diffusive boundary layer around marine animals in an ocean changing in temperature (T) and CO_2 concentration in order to compare the challenges posed by O_2 uptake under stress with the equivalent problem of CO_2 expulsion. The problem is more complex than that for a non-reactive gas since, as with gas exchange of CO_2 at the air-sea interface, the influence of the ensemble of reactions within the CO_2-HCO_3^--CO_3^{2-} acid-base system needs to be considered. These reactions significantly facilitate CO_2 efflux compared to O_2 intake at equal temperature, pressure and flow rate under typical oceanic concentrations.The effect of these reactions can be described by an enhancement factor. For organisms, this means mechanically increasing flow over their surface to thin the boundary layer as is required to alleviate O_2 stress seems not necessary to facilitate CO_2 efflux. Nevertheless the elevated pCO_2 cost most likely is non-zero. Regionally as with O_2 the combination of T, P, and pH/pCO_2 creates a zone of maximum CO_2 stress at around 1000 m depth. But the net result is that, for the problem of gas exchange with the bulk ocean, the combination of an increasing T combined with declining O_2 poses a greater challenge to marine life than does increasing CO_2. The relationships developed here allow a more accurate prediction of the impacts on marine life from the combined effects of changing T, O_2, and CO_2 than can be estimated from single variable studies.

1 Introduction

Modern climate change concerns over ocean chemical impacts arise from two primary issues: metabolic/respiratory stress imposed by rising temperature and the inevitably associated decline in dissolved O_2 (Shaffer et al., 2009), and the impacts of ocean acidification on both calcification and the more general systemic metabolic stress (Caldeira et al., 2005). In a companion paper (Hofmann et al., 2012) we addressed the problem of changing T and O_2 in terms of gas uptake rates across the animal respiratory surface diffusive boundary layer for typical oceanic profiles with depth. Here we describe the related problem for the required CO_2 export that must over time match the equivalent O_2 import.

The rise in concern over ocean acidification from the invasion of fossil fuel CO_2 (e.g., Caldeira and Wickett, 2003, 2005; Royal Society, 2005; Blackford and Gilbert, 2007; Meehl et al., 2007; IPCC, 2007; Zeebe et al., 2008) has lead to increased attention to the potential impact of elevated ocean CO_2 levels on marine animals. The early plans for direct ocean CO_2 sequestration, first advocated by Marchetti (1977), as a means of mitigating the impacts of climate change drew little attention. But as plans for experimental testing of this scheme at a site off Hawaii surfaced opposition soon arose (Haugan, 2003). The first expressions of this from the general public were unspecific and the scientific community soon realized that far too little authoritative information was available (Kita and Ohsumi, 2004). The early laboratory experiments that were carried out showed impacts of elevated CO_2 (low pH) on calcification in marine species (Gattuso et al., 1998), and potential coralline impacts are today a major field of scientific study (Orr et al., 2005).

The first small-scale experimental field test of true deep-sea CO_2 injection (Brewer et al., 1999) aroused great interest and was important in resolving numerous complex physicochemical issues such as the role of hydrate formation and the lifetime and fluid dynamics of the material. Images of a deep-sea fish swimming within a few centimeters

of the released liquid CO_2 drew attention, and general concerns over possible sublethal stress on deep-sea animals quickly became a matter of debate.

Seibel and Walsh (2001, 2003) reviewed the existing literature and inferred that impaired physiological performance would occur for many deep-sea animals under elevated CO_2 levels and noted in particular that "oxygen transport proteins are highly sensitive to changes in pH". The matter of deep-sea CO_2 injection was carefully evaluated in a major IPCC report (Caldeira et al., 2005) and the concern that deep-sea animals "would experience serious problems in oxygen supply under conditions of increased CO_2 concentrations" was reiterated; but a numerical framework within which to address this was not reported. The possible linkage between O_2 and CO_2 impacts on the functioning of marine animals remains to be formally addressed.

The challenge today is to find ways to combine the effects of simultaneous changes in T, O_2, and CO_2 within the same conceptual and numerical framework so that more quantitative estimates of impacts can be made. The result of long term changes in the ocean's oxygen status under global warming have been modeled by Shaffer et al. (2009) who concluded that the suboxic ($\leq 10\,\mu mol\,O_2\,kg^{-1}$) and hypoxic ($\leq 80\,\mu mol\,kg^{-1}$) oceanic regions would greatly expand. The long term evolution of the coupled atmospheric and oceanic thermal and CO_2 signals under various scenarios has been extensively modeled (e.g., Sarmiento and Toggweiler, 1984; Siegenthaler and Wenk, 1984; Sarmiento et al., 1995; Archer et al., 1998; Archer, 1999; Sabine et al., 2004; Archer, 2005; IPCC, 2007; Archer et al., 2009; Allen et al., 2009; Allison et al., 2009). But the impact of these combined effects on marine life remains uncertain.

Here we analyze the physical limits that apply, and by the use of simple physical and thermodynamic relationships we shed important light on the differing thermodynamic efficiencies of the mechanisms and routes taken by the O_2 and CO_2 molecules as they exchange in the boundary between the animal and the bulk fluid. In order to minimize respiratory acidosis and associated detrimental effects (e.g., Perry et al., 2010) as a result of CO_2 build-up inside an animal it is obvious that CO_2 must be exported from the cell to keep the respiration reaction energetically favorable and efficient. To

maintain mass balance, the rate of CO_2 export must be stoichiometrically related to O_2 consumption. By analyzing the process by which CO_2 is transferred from the outer membrane through the diffusive boundary layer to the bulk ocean it is possible to better evaluate the relative impacts of O_2 and CO_2 stress and more accurately predict the impacts of climate-ocean CO_2 changes on marine life.

In this paper, we investigate the diffusive limitation of CO_2 export as compared to the equivalent diffusive limitation of O_2 uptake, which we have reported in a companion paper Hofmann et al. (2012).

It is important to note that we are not addressing here the internal impacts on animal chemical functioning. We simply ask the question of whether, when faced with external CO_2 levels that could impair function, the animal must resort to increasing physical flow over the surface, or whether the same boundary layer thickness required for O_2 import is still sufficient to support the equivalent, ocean chemistry enhanced, CO_2 export.

2 Materials and methods

2.1 The oceanic CO_2 removal potential RP_{CO_2}

2.1.1 Boundary layer CO_2 diffusion with no reaction

As a first order approximation, the CO_2 efflux from an organism that consumes oxygen at a rate of E^{O_2} (in $\mu mol\,s^{-1}\,cm^{-2}$) can be defined as

$$E^{CO_2} = E^{O_2} \tag{1}$$

with the directions of the fluxes being opposite to each other.

We treat diffusion and CO_2 reactivity in seawater in two separate steps. First, we assume no CO_2 reactivity in seawater, and consider only the theoretical, purely diffusive CO_2 export flux: $E^{CO_2}_{diff}$. Following the same reasoning as in the companion paper (Hofmann et al., 2012) treating diffusive O_2 uptake limitations, we consider a step-wise

process of diffusion through the respiratory tissue and the diffusive boundary layer (DBL) in contact with this tissue. We define a transfer time for each step and, by taking the inverse of these times, define a term for the total diffusion-only CO_2 export flux (in $\mu mol\,s^{-1}\,cm^{-2}$) from the organism as

$$E^{CO_2}_{diff} = 1 \Big/ \left(\frac{1}{E^{CO_2}_{diff,\,DBL}} + \frac{1}{E^{CO_2}_{diff,\,tissue}} \right) \tag{2}$$

with

$$E^{CO_2}_{diff,\,DBL} = \frac{D^{CO_2}\,\rho_{SW}}{L^{CO_2}\,K0'^{CO_2}}\,\Delta pCO_2|_{DBL} \tag{3}$$

where ρ_{SW} is the in situ density of seawater (calculated according to Millero and Poisson, 1981, as implemented in Hofmann et al., 2010) in $kg\,cm^{-3}$, and where $K0'^{CO_2}$ is the apparent Henry's constant for CO_2 in $mol\,kg^{-1}\,atm^{-1}$ (= $\mu mol\,kg^{-1}\,\mu atm^{-1}$) at in-situ conditions

$$K0'^{CO_2} = \frac{[CO_2]}{pCO_2([CO_2],T,S,P)} \tag{4}$$

$[CO_2]$ in $mol\,kg^{-1}$ here is an arbitrary concentration and in the denominator pCO_2 in atm is first calculated in the conventional way from $[CO_2]$ using the common mass unit Henry's constant $K0$, calculated according to Weiss (1974) using potential temperature (θ, Bryden, 1973; Fofonoff, 1977), and the fugacity coefficient for CO_2 calculated as given in Zeebe and Wolf-Gladrow (2001) (restated from Koertzinger, 1999). Resulting pCO_2 values are then corrected for hydrostatic pressure (calculated from given depth values according to Fofonoff and Millard, 1983) according to Enns et al. (1965).

Again, as in (Hofmann et al., 2012), we now consider the external physical constraints on respiratory gas exchange imposed by the surrounding ocean, which means

$E^{CO_2}_{tissue} >> E^{CO_2}_{DBL}$. This implies that the total flux $E^{CO_2}_{diff}$ approaches $E^{CO_2}_{DBL}$ and Eq. (2) can be restated as

$$E^{CO_2}_{diff} \leq \frac{D^{CO_2}\,\rho_{SW}}{L^{CO_2}\,K0'^{CO_2}}\,\Delta pCO_2|_{DBL} \tag{5}$$

2.1.2 Boundary layer CO_2 reactivity: the enhancement factor EF

In contrast to the O_2 case, CO_2 is reactive in seawater via acid-base equilibration reactions of the carbonate system (e.g., Zeebe and Wolf-Gladrow, 2001), the most important ones being

$$CO_2 + H_2O \longleftrightarrow HCO_3^- + H^+ \tag{6}$$

$$CO_2 + OH^- \longleftrightarrow HCO_3^- \tag{7}$$

While these reactions and other aquatic acid-base equilibration reactions can be treated in great detail (e.g., Hofmann et al., 2008, 2010), very reasonable approximations (Emerson, 1975; Zeebe and Wolf-Gladrow, 2001) give a dimensionless "enhancement factor" EF that well describes the enhancement of diffusive CO_2 transport by the above reactions

$$\mathrm{EF} = \frac{E^{CO_2}}{E^{CO_2}_{diff}} = f(L^{CO_2}, T, S, P, \mathrm{pH_{free\ scale}}) \tag{8}$$

where E^{CO_2} represents the true CO_2 flux including the effect of chemical reactions and $E^{diff}_{CO_2}$ is the hypothetical diffusive flux that would occur if CO_2 were not chemically reactive in seawater, as described in Sect. 2.1.1. The dimensionless factor EF is a function

of the thickness of the diffusive boundary layer for CO_2, L^{CO_2} in cm, temperature T in °C, salinity S, hydrostatic pressure P in bar, and the ambient pH on the free scale $\mathrm{pH_{free\ scale}}$. It can be calculated for plane geometry, which is here used as a first order approximation for any biologic gas exchange surface, as

$$\mathrm{EF} = \frac{L^{CO_2}}{a_k}\,\coth\left(\frac{L^{CO_2}}{a_k}\right) \tag{9}$$

with = a_k in cm being the reacto-diffusive length scale for CO_2 diffusion and the reactions given in Eqs. (6) and (7), which can be calculated as

$$a_k = \sqrt{\frac{D^{CO_2}}{k_{+1} + k_{+4}\,[OH^-]}} \tag{10}$$

Again, the molecular diffusion coefficient for CO_2 in $\mathrm{cm^2\,s^{-1}}$, D^{CO_2}, can be calculated as a function of S, T, and P. k_{+1} is the forward rate constant in $\mathrm{s^{-1}}$ of the reaction of CO_2 and H_2O (Eq. 6) and k_{+4} is the forward rate constant in $\mathrm{kg\,mol^{-1}\,s^{-1}}$ of the reaction of CO_2 and OH^- (Eq. 7), both can be calculated (k_{+1} and k_{+4} are here calculated as given in Zeebe and Wolf-Gladrow (2001) as functions of temperature T. $[OH^-]$ is the hydroxyl ion concentration in $\mathrm{mol\,kg^{-1}}$ calculated as

$$[OH^-] = \frac{K_W}{10^{-\mathrm{pH_{free\ scale}}\,\frac{\mathrm{mol}}{\mathrm{kg}}}} \tag{11}$$

where K_W in $\mathrm{mol^2\,kg^{-2}}$ is the ion product of water, calculated (K_W is here calculated after Millero (1995) as implemented in Hofmann et al. (2010)) as a function of temperature T and salinity S.

Note that Zeebe and Wolf-Gladrow (2001) also define a "spherical" version of EF which is meant for microorganisms where the effective thickness of the DBL (i.e., L^{CO_2}

here) is equal to the radius of the sphere (e.g., Zeebe and Wolf-Gladrow, 2001). While being a valuable description for plankton and unicellular algae, for any other (i.e., macroscopic) organism, the planar description is more appropriate: while there will be a specific description for each animal shape, gas exchange tissue shape and size, mode of swimming and pumping etc., there will always be a dependency on the flow velocity across the gas exchange tissue. The planar surface description is the most generic and widely applicable description that allows for such a parameterization. It is also given in this form in Zeebe and Wolf-Gladrow (2001), and therefore we use it here.

Using EF we can write an equation for the CO_2 export flux from an organism (in $\mu mol\,s^{-1}\,cm^{-2}$), considering both diffusion and CO_2 reactivity in seawater

$$E^{CO_2} = E^{CO_2}_{diff}\,EF \tag{12}$$

Using Eq. (2), for $E^{CO_2}_{diff}$, this means

$$E^{CO_2} \leq \frac{D^{CO_2}\,\rho_{SW}\,K0'^{CO_2}\,EF}{L^{CO_2}}\,\Delta pCO_2|_{DBL} \tag{13}$$

2.1.3 Defining RP_{CO_2} equivalently to SP_{O_2}

In order to define a quantity similar to the oceanic oxygen supply potential SP_{O_2} in the oxygen companion paper (Hofmann et al., 2012), we now divide both sides of the equation by the DBL thickness L^{CO_2} (For O_2 this results in a purely oceanic property that is independent of any animal specific boundary layer thickness; however the chemical reactivity of the CO_2 molecule within the boundary layer prohibits such simplification here although we show that a close approximation is possible).

$$E^{CO_2}\,L^{CO_2} \leq D^{CO_2}\,\rho_{SW}\,K0'^{CO_2}\,EF\,\Delta pCO_2|_{DBL} \tag{14}$$

Considering the limiting case, i.e., the maximal upper boundary for the CO_2 removal rate, we can now define the oceanic CO_2 removal potential (in $\mu mol\,s^{-1}\,cm^{-1}$) as

$$RP_{CO_2} := D^{CO_2}\,\rho_{SW}\,K0'^{CO_2}\,EF\,\Delta pCO_2|_{DBL} \tag{15}$$

However, as opposed to the O_2 case, where SP_{O_2} is independent of the description of the DBL used, i.e., the DBL thickness L, here, EF is a function of L^{CO_2}, which means RP_{CO_2} depends on a model description for the DBL. Again, we use a generic planar surface description as given in Table 1 (adapted for CO_2 from Hofmann et al. (2012)).

While the term RP_{CO_2} itself does depend on the DBL properties, RP_{CO_2} with EF = 1 can be interpreted as a "purely diffusive" oceanic CO_2 removal potential, a quantity that is not dependent on a DBL model description. The more realistic quantity with real physico-chemical meaning, however, is RP_{CO_2} with EF as calculated above in Eq. (9). We point out that the boundary layer property L^{CO_2}-description here (as well as the planar EF description) is meant for large scale oceanic comparison only and appropriate values can and should be substituted for organism and system specific descriptions if this is desired. The sensitivity of our calculations with respect to fluid flow velocities are explored below.

RP_{CO_2} depends on the CO_2 partial pressure differential $\Delta pCO_2|_{DBL} = \left(pCO_2|_s - pCO_2|_f\right)$ across the DBL with $pCO_2|_f$ being the ambient free stream pCO_2 value and $pCO_2|_s$ being the pCO_2 value directly at the organism surface. Here, we investigate outer envelopes of diffusive CO_2 export limitations, i.e., we are interested in maximal values for RP_{CO_2}. $\Delta pCO_2|_{DBL}$ and thus RP_{CO_2} are maximal when $pCO_2|_s$ is maximal.

2.1.4 $pCO_2|_s^{max}$, an exemplary maximal value for the CO_2 partial pressure in molecular contact with an organism

The sensitivity of marine animals to elevated internal pCO_2 levels varies with species and life stage. Absolute limits are hard to define, as knowledge about the effects of

acute hypercapnia is still limited (see, e.g., Caldeira et al., 2005; Poertner et al., 2005). Almost nothing is know about the limits for pCO_2 or pH in diffusive molecular contact with the outside of the gas exchange surface of an organism. However, to calculate maximal RP_{CO_2} values, Eq. (15) requires a maximal value for $pCO_2|_s$, which exactly represents this maximal pCO_2 directly at the (gas exchange) surface of an organism. For the example calculations given here, comparing various oceanic regions amongst each other, we use one single, constant value $pCO_2|_s = pCO_2|_s^{max} = 5000\,\mu atm$. If attained in the external medium, this pCO_2 would produce effects such as narcosis and mortality in sensitive organisms (Caldeira et al., 2005).

Since, a certain limit pCO_2 value in the free stream entails a higher pCO_2 value in molecular contact with the organism surface, and effects for $pCO_2 = 5000\,\mu atm$ are reported in Caldeira et al. (2005) for only the most sensitive organisms, choosing $pCO_2|_s = pCO_2|_s^{max} = 5000\,\mu atm$ is a rather low estimate for a limit value, likely overestimating the CO_2 removal limitation in our calculations.

While we are aware that $pCO_2|_s = pCO_2|_s^{max} = 5000\,\mu atm$ is an assumption serving mainly exemplary purposes here, using one single constant value effectively also removes species dependency from the calculation of RP_{CO_2}. The calculation may easily be repeated by substituting known species specific values. The sensitivity of our calculations with respect to $pCO_2|_s$ are explored below.

2.2 Maximal CO_2 diffusion limited metabolic rate $E_{max}^{CO_2}$

Analogous to the oxygen quantity E_{max} (Hofmann et al., 2012), we can define a maximal metabolic rate (CO_2 export and thus O_2 import) that diffusive limitation of CO_2 export would allow

$$E_{max}^{CO_2} := \frac{RP_{CO_2}}{L^{CO_2}} = \frac{D^{CO_2}\,\rho_{SW}\,K0'^{CO_2}\,EF}{L^{CO_2}}\,\Delta pCO_2|_{DBL} \tag{16}$$

Here, we use the same generic description for L^{CO_2} (given in Table 1) as used for the EF definition (Eq. 9).

2.3 Required $\Delta pCO_2|_{DBL}$ for a given E_{O2}

Similar to the O_2 quantity C_f (Hofmann et al., 2012), we can define a quantity that is not dependent on the external CO_2 content of the water. To explicitly include the dependence of gas exchange on partial pressure and the dependency of partial pressure on hydrostatic pressure (Enns et al., 1965), we assume a given oxygen uptake rate E^{O_2} (in $\mu mol\,s^1\,cm^2$), experimentally determined at diffusivities and DBL thicknesses equal to the respective in-situ values, but at one atmosphere.

As stated in Eq. (1), we assume $E_{CO_2} = E^{O_2}$, with the flux directions defined as opposite. Therefore, we can calculate the required CO_2 partial pressure differential (in µatm) that is able to support a given metabolic rate (O_2 import and thus CO_2 export) by making use of Eq. (13)

$$\Delta pCO_2|_{DBL} \geq \frac{E^{O_2}\,L^{CO_2}}{D^{CO_2}\,\rho_{SW}\,K0'^{CO_2}_{E\text{—}EF}} \tag{17}$$

where $K0'^{CO_2}_E$ is the apparent Henry's constant (calculated as eluded to above) at "experimental" conditions, i.e., at the conditions at which E_{O_2} was determined, most notably one atmosphere. Again, considering the limiting case of a minimal partial pressure differential that satisfies Eq. (17), we can define

$$\Delta p_{DBL} := \frac{E^{O_2}\,L^{CO_2}}{D^{CO_2}\,\rho_{SW}\,K0'^{CO_2}_E\,EF} \tag{18}$$

For exemplary purposes, we use $E^{O_2} = 20 \times 10^{-7}\,\mu mol\,s^{-1}\,cm^{-2}$, consistent with the oxygen companion paper Hofmann et al. (2012).

2.4 Required minimal $pCO_2|_s$ for given external conditions and given E^{O_2}

Having calculated the minimally required pCO_2 gradient Δp_{DBL} to sustain a given E^{O_2} (and associated E^{CO_2}) from Eq. (18), a minimally required pCO_2 (in µatm) in molecular contact with the gas exchange surface of the organism can be calculated by using a given, pressure corrected (Enns et al., 1965) free stream (i.e., bulk ocean) CO_2 partial pressure $pCO_2|_f$

$$pCO_2|_s^{min} = pCO_2|_f + \Delta p_{DBL} \quad (19)$$

2.5 Maximal $pCO_2|_f$ for given E^{O_2} and assumed $pCO_2|_s$

Similarly, the maximal external free stream pCO_2 permitting the efflux required for metabolic balance can be calculated. If the (maximal) CO_2 partial pressure $pCO_2|_s$ in contact with the respiratory surface that permits normal functioning of the animal is given, then

$$pCO_2|_f^{max} = pCO_2|_s - \Delta p_{DBL} \quad (20)$$

For illustrative purposes, we again assume $pCO_2|_s = pCO_2|_s^{max} = 5000$ µatm for calculations here.

2.6 Limiting external conditions for given E^{O_2} and assumed $pCO_2|_s$

The quantity $pCO_2|_f^{max}$ can then be used to calculate the maximal, in situ, CO_2 concentration in the free stream bulk medium that is required for an experimentally observed O_2 demand to be supported as in

$$[CO_2]_f^{max} = pCO_2|_f^{max} K0'^{CO_2} \quad (21)$$

where $K0'^{CO_2}$ in mol kg^{-1} atm^{-1} is the apparent in-situ Henry's constant as calculated above (Eq. 4).

The property $[CO_2]_f^{max}$ can then be used to calculate limiting bulk fluid ocean conditions (e.g., maximal $[\sum CO_2]$: $[\sum CO_2]_f^{max}$, minimal total scale pH: $pH|_f^{min}$, etc.) that can balance the required O_2 consumption. Bulk fluid free stream conditions here are calculated in the programming language R with the acid-base chemistry routines implemented in the R extension package AquaEnv (Hofmann et al., 2010), with the Millero et al. (2006) equilibrium constants for the carbonate system and all other constants being the standard AquaEnv formulations with references given there. $[\sum(BOH)_3]$, $[\sum H_2SO_4]$, and $[\sum HF]$ are estimated from salinity S as given in DOE (1994) and Dickson et al. (2007). Conversions between free scale and total scale pH are done as implemented in AquaEnv.

2.7 External conditions: present-day and future values

In order to compare our derived example limiting free-stream conditions (maximal pCO_2, $[\sum CO_2]$, and minimal pH) to present-day conditions we use data from the alkalinity and dissolved inorganic carbon climatology of Goyet et al. (2000) for a location off the coast of Southern California (SC: 120.5° W, 29.50° N) and other stations around the world (CH: Chile (75.5° W, 33.5° S); WP: Western Pacific (126.5° E, 11.5° N), WA: Western Africa (6.5° E, 15.5° S), MD: Mediterranean (18.5° E, 35.5° N); BB: Bay of Bengal (87.5° E, 18.5° N)), consistent with the oxygen companion paper Hofmann et al. (2012). Particularly, the southern California region is selected since it is well studied, and the eastern Pacific region shows strong vertical gradients in both O_2 and CO_2, thus ecompassing a wide range of oceanic values.

For future conditions we note that atmospheric pCO_2 may approximately triple from pre-industrial by the end of the century (e.g., IPCC, 2007; Meehl et al., 2007) with well predicted oceanic CO_2 system consequences (e.g., Zeebe et al., 2008; Allison et al., 2009). We therefore assume a tripled pCO_2 at all depths with associated increase in $[\sum CO_2]$ and decrease in pH, assuming constant alkalinity while recognizing that it will

take several hundred years given the slow pace of oceanic mixing for changes of such scale to appear at depth.

3 Results and discussion

3.1 Sensitivity of RP_{CO_2} and $E_{max}^{CO_2}$ with respect to u_{100} and $pCO_2|_s^{max}$

Figure 1 shows various plots that investigate the sensitivity of the two central derived quantities RP_{CO_2} and $E_{max}^{CO_2}$ with respect to the input parameters u_{100} and $pCO_2|_s^{max}$. Both parameters are not accessible via typical oceanographic data and our calculations rely on assumed constant values for those parameters. Fig. 1 illustrates how our derived quantities depend on those input parameters and what the assumed values for them entail.

The left panel in the upper row of Fig. 1 shows that the EF dependency on u_{100} is dominated by the dependency of the DBL thickness L^{CO_2} on u_{100} (see Table 1 and the companion paper Hofmann et al. (2012) for details). Since RP_{CO_2} depends linearly on EF (cf. Eq. 15), the EF dependency on u_{100} exactly mirrors the RP_{CO_2} dependency on u_{100} (not shown).

EF increases with increasing temperature, rougly two-fold for a temperature increase from 1 °C to 25 °C (top left panel of Fig. 1). The general dependency of EF on u_{100} is not affected by temperature.

The central panel in the top row of Fig. 1 shows that RP_{CO_2} increases by about an order of magnitude in the u_{100} range sampled, with the largest steps being exhibited for small u_{100}, which is consistent with the steep part of the curve of the EF dependency on u_{100} for u_{100} values below approximately 3 cm s^{-1}.

The case of EF = 1 completely eliminates the dependency of RP_{CO_2} on u_{100}, but is equivalent to very large values of u_{100}. Consistently, the lowest values for RP_{CO_2} are obtained with EF = 1.

The right panel in the top row of Fig. 1 illustrates the linear dependency of RP_{CO_2} on the CO_2 partial pressure limit value in molecular contact with the organism ($pCO_2|_s = pCO_2|_s^{max}$). RP_{CO_2} values increase from about 2×10^{-6} µmol s^{-1} to about 20×10^{-6} µmol s^{-1}, when $pCO_2|_s^{max}$ increases from 2000 µatm to 20 000 µatm.

The better quantity to look at, however, when assessing the influence of the fluid flow velocity u_{100} on the ability of the ocean to remove respiratory CO_2 from the organism is the quantity $E_{max}^{CO_2}$. RP_{CO_2} depends on EF which decreases with increasing u_{100}, i.e., in a thinner boundary layer, there is less time for the CO_2 acid-base system to convert CO_2 to carbonate and bicarbonate and thus effectively remove CO_2 itself which enhances diffusion. However, RP_{CO_2} does not incorporate the fact that with a thinner boundary layer, there is a shorter way for the CO_2 to diffuse through, since the DBL thickness L^{CO_2} is removed from the definition to be consistent with the oxygen quantity SP_{O_2} in the companion paper. The quantity $E_{max}^{CO_2}$, however, does include this effect. The left panel in the bottom row of Fig. 1 shows that $E_{max}^{CO_2}$ increases steeply with increasing u_{100}, once u_{100} has values above approximately 3 cm s^{-1}. Below a free stream velocity of 3 cm s^{-1}, $E_{max}^{CO_2}$ is virtually independent of u_{100}. For u_{100} values larger than 5 cm s^{-1} the relation is almost linear. The overall positive correlation of $E_{max}^{CO_2}$ with u_{100} shows that the effect of increasing flow decreasing the distance for diffusion (L^{CO_2} decreases with increasing u_{100}, which increases $E_{max}^{CO_2}$) dominates over the effect that this decreased distance allows for less time for the CO_2 system to enhance the diffusive flux via chemical reactions (EF decreases with increasing u_{100}, which decreases $E_{max}^{CO_2}$).

$E_{max}^{CO_2}$ increases with increasing temperature, also about two-fold for a temperature increase from 1 °C to 25 °C (bottom left panel of Fig. 1). It can be seen that the dependency of $E_{max}^{CO_2}$ on u_{100} is less pronounced for higher temperatures.

Comparing the central panels in upper and bottom rows of Fig. 1 illustrates the difference in DBL thicknes L^{CO_2} (i.e., u_{100}) dependency of RP_{CO_2} and $E_{max}^{CO_2}$. While RP_{CO_2} shows a strong negative correlation with u_{100} (central panel, top row Fig. 1), $E_{max}^{CO_2}$, exhibits a moderate positive correlataion with u_{100}. As already mentioned above, the effect of less distance for diffusion with increasing u_{100} outweighs the effect of less time for chemical enhancement of the flux with increasing u_{100}. However, due to the combination of those two counteracting effects, the net dependency of $E_{max}^{CO_2}$ on u_{100} is much less pronounced than the dependency of RP_{CO_2} on u_{100} and also the dependency of SP_{O_2} (Hofmann et al., 2012) on u_{100}. In the central panel of the bottom row of Fig. 1, it can also clearly be seen that the dependency of $E_{max}^{CO_2}$ on u_{100} is less pronounced at shallower depths with higher temperatures and pH values than at deeper depths with colder temperatures and lower pH values.

In the case of EF = 1, one assumes an effect of u_{100} on L^{CO_2}, i.e., decreasing the distance for diffusion with increasing flow velocity, but the effect of chemical enhancement in a thick DBL is neglected. Therefore, the EF = 1 case here shows the lowest values for $E_{max}^{CO_2}$ although for the calculation of L^{CO_2} an intermediate value of 6 cm s^{-1} is used for u_{100}.

The right panel in the bottom row of Fig. 1 shows that the dependency on $pCO_2|_s^{max}$ is similar for $E_{max}^{CO_2}$ and RP_{CO_2}.

3.2 Example depth profiles for various stations around the world

Figure 2 shows RP_{CO_2} depth profiles for example stations around the world (top panels) It can be clearly seen, that the profiles are overall dominated by the enhancement factor (bottom panels), which exhibits rather similar values for deeper depths between all profiles, but differs for depths shallower then 500 m due to different temperature and pH profiles (due to its dependency on [OH^-], EF depends positively on pH, see Eq. 9 to 11.) This dependency of EF on pH is also the reason for the fact that the profile for the

Mediterranean (MD) shows markedly higher EF and thus RP_{CO_2} values than profiles for the other stations, as the mediterranean profile exhibits higher alkalinity (central panels of Fig. 3) and thus lower pCO_2 (bottom panels of Fig. 3) and higher pH (not shown).

The specific shapes of and the differences between RP_{CO_2} profiles, especially at deeper depths, is caused by differing pCO_2 profiles, as the central panels of Fig. 4 (RP_{CO_2}, with EF = 1) show when compared to pCO_2 profiles of the respective stations (bottom panels of Fig. 3). Off the coast of Chile (station CH), a clear pCO_2 maximum can be identified shallower than 500 m (bottom left panel of Fig. 3), which results in a local dip in RP_{CO_2} values (top left panel of Fig. 2), and which is due to a local [$\sum CO_2$] maximum (top left panel of of Fig. 3). This region corresponds to the local oxygen minimum in this region as described in the companion paper Hofmann et al. (2012).

Figure 4 shows $E_{max}^{CO_2}$ depth profiles. As expected, the general shape of the profiles is the same as for RP_{CO_2}, as $E_{max}^{CO_2}$ is calculated by dividing RP_{CO_2} by L^{CO_2} which is calculated using a constant u_{100} of 6 cm s^{-1}.

The top panels of Fig. 5 show depth profiles of Δp_{DBL}, the CO_2 partial pressure differential across the DBL that is required to sustain a given oxygen uptake and resulting CO_2 export. It can clearly be seen, that Δp_{DBL} decreases with depth and decreasing temperature. The Δp_{DBL} profiles are rather similar for all stations, with a pronounced difference for the Mediterranean (MD) station, most likely due to high temperatures and [TA] values (see also Fig. 3).

In the bottom panels of Fig. 5 depth profiles of $pCO_2|_s^{min}$, the minimal CO_2 partial pressure in molecular contact with the organism surface that is required to drive a given metabolic flux across the DBL, are given. The general shape of the profiles are dominated by ambient pCO_2 profiles (Fig. 3), but for all stations except the Mediterranean station (MD), values at depth are considerably higher for $pCO_2|_s^{min}$ than for ambient pCO_2 due to the higher Δp_{DBL} values caused by lower temperatures.

3.3 Diffusive CO_2 limitation? Present and future conditions

Having calculated a $pCO_2|_f^{max}$ (the maximal pCO_2 in the free stream that can support a given metabolic rate) profile for the Southern California (SC) station, we calculated limiting external conditions from that: the maximal external dissolved inorganic carbon concentration $[\sum CO_2]_f^{max}$, and the minimal free stream, total scale pH $pH|_f^{min}$. Figure 6 shows profiles of those external limit conditions (black lines) and compares them to present-day ambient conditions extracted from the Goyet et al. (2000) climatology (blue lines). It can be seen that present-day ambient conditions are rather far away from the calculated limit conditions. However, crudely assumed future conditions (i.e., a tripling of pCO_2 in the whole water column by appropriate theoretical addition of dissolved inorganic carbon), show that there is a region at about 700 m depth at this station, where diffusive CO_2 export could become close to limiting, given the assumed metabolic rate of $E^{O_2} = 20 \times 10^{-7}$ µmol s^{-1} cm^{-2}.

3.4 Diffusive CO_2 limitation vs. diffusive O_2 limitation

Figure 7 compares depth profiles for the Southern California station (SC) of the equivalent diffusive oxygen and carbon dioxide limitation quantities SP_{O_2} and RP_{CO_2}, as well as $E_{max}^{O_2}$ (called E_{max} in Hofmann et al., 2012) and $E_{max}^{CO_2}$.

The left panel of Fig. 7 compares SP_{O_2} (red line) and RP_{CO_2}, calculated with a fluid flow velocity of 2 cm s^{-1} (black line). SP_{vO_2} values are considerably lower than RP_{CO_2} values throughout the whole water column, suggesting that diffusive limitation of oxygen uptake is dominant over diffusive limitation of respiratory carbon dioxide export. Comparing present-day SP_{O_2} values with RP_{CO_2} calculated with assumed future conditions (i.e., a tripled pCO_2 throughout the whole water column, blue line), still reveals a dominance of diffusive oxygen limitation over diffusive carbon dioxide export limitation. And this is without assuming any decline in oceanic oxygenation, which would decrease SP_{O_2} values even further and would thus amplify the dominance of oxygen

limitaion over carbon dioxide limitation. It must be noted, however, that, although both quantities are defined as equivalent as possible, RP_{CO_2} still depends on the free stream water velocity u_{100} via the enhancement factor EF. RP_{CO_2} values here are calculated with the rather low velocity of 2 cm s^{-1}, to assume a rather high diffusive CO_2 limitation, yet, SP_{O_2} and RP_{CO_2} are not optimal quantities when comparing diffusive oxygen uptake limitation to diffusive carbon dioxide export limitation.

The better quantity-pair to this end is the pair $E_{max}^{O_2}$ and $E_{max}^{CO_2}$, as both quantities similarly depend on the free stream water velocity, and if the same DBL model description is used for both quantities, a relative comparison between both quantities will be valid and meaningful. The right panel of Fig. 7 compares $E_{max}^{O_2}$ and $E_{max}^{CO_2}$ values calculated with different free stream water velocities u_{100}. Even comparing $E_{max}^{O_2}$ values calculated with $u_{100} = 6$ cm s^{-1} (orange line), to $E_{max}^{CO_2}$ values calculated with $u_{100} = 2$ cm s^{-1}, which artificially favors CO_2 limitation, confirms the dominance of diffusive oxygen uptake limitation over diffusive carbon dioxide export limitation. Only $E_{max}^{CO_2}$ values calculated with a future tripled pCO_2 and 2 cm s^{-1} (red line) are close to $E_{max}^{O_2}$ values calculated with 6 cm s^{-1} (orange line), which is an artificial case, strongly favoring CO_2 limitation.

Important to note is that the value for $pCO_2|_s$ used here is deliberately chosen to be comparatively low, i.e., only the most sensitive organisms show reactions in Caldeira et al. (2005), so that the defined CO_2 limiting quantities likely overestimate the CO_2 removal limitation. So when compared to the equivalent oxygen supply limitation quantities, highest conceivable CO_2 export limitations are considered. Still, diffusive oxygen uptake limitation seems to be dominant, due to the chemical enhancement of the diffusive CO_2 export.

4 Conclusions and outlook

The ocean is now undergoing simultaneous warming, loss of O_2, and rising CO_2 levels. The impact of changes in each of these properties draws intense scientific scrutiny but ways in which the ensemble effect can be estimated are few. In a first attempt to address the combined impacts Brewer and Peltzer (2009) defined a "respiration index" which linked the ratios of pO_2 to pCO_2 via the simple form of the Gibbs' free energy equation. This paper, by converting traditional properties such as a simple mass values for $[O_2]$ into the partial pressures that can accommodate changing temperature and correctly represent the driving force for respiration, is an attempt to assess the relative hospitability of certain ocean regions to support aerobic respiration (e.g., Mayol et al., 2012).

Our findings here, and in the oxygen companion paper, that it is energetically easier to transport CO_2 away from an organism due to the chemical enhancement term than to bring O_2 towards it which requires physical changes in diffusive boundary layer thickness, suggests a route towards an improved function. In this function, estimating only physical processes originating in the external ocean, declines in pO_2 would be given more weight than increases in pCO_2.

Although neither impact is positive for marine life, considering only diffusive limitation effects, global warming/declining O_2 is most likely a greater threat to most oceanic life than is oceanic uptake of antropogenic CO_2. However, there might be further respiratory effects of CO_2 input and acidification that are not considered here: such as oxygen transport mechanisms in animals are impacted by an elevated proton concentration (e.g., Seibel and Walsh, 2003) and the decrease of the free energy yield of the respiration reaction (Brewer and Peltzer, 2009).

Of course, as already widely studied and well known, ocean acidification due to anthropogenic CO_2 uptake of the oceans results in a decrease in the carbonate ion concentration with negative effects on biogenic calcification. Animals will have to expend energy in an effort to reduce the loss of carbonate shell protection. This means

O_2 dependent processes will have to be increased, in principle favoring non-calcifying organisms in high CO_2 low O_2 regions, and thus establishing a more direct linkage between O_2 and CO_2 in the ocean.

Acknowledgements. This work was supported by a grant to the Monterey Bay Aquarium Research Institute from the David & Lucile Packard Foundation.

References

Allen, M. R., Frame, D. J., Huntingford, C., Jones, C. D., Lowe, J. A., Meinshausen, M., and Meinshausen, N.: Warming caused by cumulative carbon emissions towards the trillionth tonne, Nature, 458, 1163–1166, doi:10.1038/nature08019, 2009. 15790

Allison, I., Bindoff, N. L., Bindschadler, R. A., Cox, P. M., de Noblet, N., England, M. H., Francis, J. E., Gruber, N., Haywood, A. M., Karoly, D. J., Kaser, G., Le Quéré, C., Lenton, T. M., Mann, M. E., McNeil, B. I., Pitman, A. J., Rahmstorf, S., Rignot, E., Schellnhuber, H. J., Schneider, S. H., Sherwood, S. C., Somerville, R. C. J., Steffen, K., Steig, E. J., Visbeck, M., and Weaver, A.: The Copenhagen Diagnosis: Updating the world on the Latest Climate Science, The University of New South Wales Climate Change Research Centre (CCRC), Sydney, Australia, 60 pp., 2009. 15790, 15800

Archer, D.: Modeling CO_2 in the Ocean: a review, in: Scaling of Trace Gas Fluxes between Terrestrial and Aquatic Ecosystems and the Atmosphere, edited by: Bouwman, A. F., 24, 169–184, Elsevier Sciences, Amsterdam, 1999. 15790

Archer, D.: Fate of fossil fuel CO_2 in geologic time, J. Geophys. Res.-Oceans, 110, C09S05, doi:10.1029/2004JC002625, 2005. 15790

Archer, D., Kheshgi, H., and Maier-Reimer, E.: Dynamics of fossil fuel CO_2 neutralization by marine $CaCO_3$, Global Biogeochem. Cy., 12, 259–276, 1998. 15790

Archer, D., Eby, M., Brovkin, V., Ridgwell, A., Cao, L., Mikolajewicz, U., Caldeira, K., Matsumoto, K., Munhoven, G., Montenegro, A., and Tokos, K.: Atmospheric Lifetime of Fossil Fuel Carbon Dioxide, Annu. Rev. Earth Pl. Sc., 37, 117–134, doi:10.1146/annurev.earth.031208.100206, 2009. 15790

Biron, P. M., Robson, C., Lapointe, M. F., and Gaskin, S. J.: Comparing different methods of bed shear stress estimates in simple and complex flow fields, Earth Surf. Proc. Land., 29, 1403–1415, doi:10.1002/esp.1111, 2004. 15814

Blackford, J. C. and Gilbert, F. J.: pH variability and CO_2 induced acidification in the North Sea, J. Mar. Syst., 64, 229–241, 2007. 15789
Boudreau, B. P.: A method-of-lines code for carbon and nutrient diagenesis in aquatic sediments, Comput. Geosci., 22, 479–496, 1996. 15814
Brewer, P. and Peltzer, E.: Limits to Marine Life, Science, 324, 347–348, 2009. 15807
Brewer, P. G., Friederich, G., Peltzer, E. T., and Orr Jr., F. M.: Direct Experiments on the Ocean Disposal of Fossil Fuel CO_2, Science, 284, 943–945, doi:10.1126/science.284.5416.943, 1999. 15789
Bryden, H. L.: New polynomials for thermal expansion, adiabatic temperature gradient and potential temperature of sea water, Deep-Sea Res., 20, 401–408, 1973. 15792
Caldeira, K. and Wickett, M. E.: Anthropogenic carbon and ocean pH, Nature, 425, 365–365, 2003. 15789
Caldeira, K. and Wickett, M. E.: Ocean model predictions of chemistry changes from carbon dioxide emissions to the atmosphere and ocean, J. Geophys. Res.-Oceans, 110, C09S04, doi:10.1029/2004JC002671, 2005. 15789
Caldeira, K., Akai, M., Brewer, P., Chen, B., Haugan, P., Iwama, T., Johnston, P., Kheshgi, H., Li, Q., Ohsumi, T., Pörtner, H. O., Sabine, C., Shirayama, Y., Thomson, J., Barry, J., and Hansen, L.: Ocean Storage, in: IPCC Special Report on Carbon dioxide Capture and Storage, IPCC, 2005. 15789, 15790, 15797, 15806
Dickson, A. G., Sabine, C., and Christian, J. R.: Guide to best practices for ocean CO_2 measurements, PICES Special Publications, 1–191, 2007. 15800
DOE: Handbook of Methods for the Analysis of the Various Parameters of the Carbon Dioxide System in Sea Water, ORNL/CDIAC-74, 1994. 15800
Emerson, S.: Chemically Enhanced Carbon Di Oxide Gas Exchange In A Eutrophic Lake A General Model, Limnol. Oceanogr., 20, 743–761, 1975. 15793
Enns, T., Scholander, P. F., and Bradstreet, E. D.: Effect of Hydrostatic Pressure on Gases Dissolved in Water, J. Phys. Chem., 69, 389–391, 1965. 15792, 15798, 15799
Fofonoff, N. P.: Computation of potential temperature of seawater for an arbitrary reference pressure, Deep-Sea Res., 24, 489–491, 1977. 15792
Fofonoff, N. P. and Millard, R. C. J.: Algorithms for computation of fundamental properties of seawater, UNESCO Technical Papers in Marine Science, 44, 55 pp., 1983. 15792
Garcia, H. E., Locarnini, R. A., Boyer, T. P., Antonov, J. I., Baranova, O. K., Zweng, M. M., and Johnson, D. R.: World Ocean Atlas 2009, Volume 3: Dissolved Oxygen, Apparent Oxy-

gen Utilization, and Oxygen Saturation., NOAA Atlas NESDIS 70, edited by: Levitus, S., US Government Printing Office, Washington, DC, 344 pp., 2010. 15821
Gattuso, J. P., Frankignoulle, M., Bourge, I., Romaine, S., and Buddemeier, R. W.: Effect of calcium carbonate saturation of seawater on coral calcification, Global Planet. Change, 18, 37–46, doi:10.1016/S0921-8181(98)00035-6, 1998. 15789
Goyet, C., Healy, R. J., and Ryan, J. P.: Global distribution of total inorganic carbon and total alkalinity below the deepest winter mixed layer depths, ORNL/CDIAC-127, NDP-076, Carbon Dioxide Information Analysis Center, Oak Ridge National Laboratory, US Department of Energy, Oak Ridge, Tennessee, 40 pp., 2000. 15800, 15805, 15815, 15816, 15817, 15818, 15819, 15820, 15821
Haugan, P. M.: On the production and use of scientific knowledge about ocean sequestration, in: Greenhouse Gas Control Technologies, edited by: Gale, J. and Kaya, Y., 1, 719–724, Proceedings of the 6th International Conference on Greenhouse Gas Control Technolgies, Elsevier, 2003. 15789
Hickey, B., Baker, E., and Kachel, N.: Suspended particle movement in and around Quinault submarine canyon, Mar. Geol., 71, 35–83, doi:10.1016/0025-3227(86)90032-0, 1986. 15814
Hofmann, A. F., Meysman, F. J. R., Soetaert, K., and Middelburg, J. J.: A step-by-step procedure for pH model construction in aquatic systems, Biogeosciences, 5, 227–251, doi:10.5194/bg-5-227-2008, 2008. 15793
Hofmann, A. F., Soetaert, K., Middelburg, J. J., and Meysman, F. J. R.: AquaEnv : An Aquatic Acid-Base Modelling Environment in R, Aquat. Geochem., 16, 507–546, 2010. 15792, 15793, 15794, 15800
Hofmann, A. F., Peltzer, E. T., and Brewer, P. G.: Kinetic bottlenecks to chemical exchange rates for deep-sea animals – Part 1: Oxygen, Biogeosciences Discuss., 9, 13817–13856, doi:10.5194/bgd-9-13817-2012, 2012. 15789, 15791, 15792, 15795, 15796, 15797, 15798, 15800, 15801, 15803, 15804, 15805, 15821
IPCC: Climate Change 2007: Synthesis Report, Contributions of Working Groups I, II, and III to the Fourth Assessment Report of the Intergovernmental Panel on Climate Change, Tech. rep., Geneva, Switzerland, 2007. 15789, 15790, 15800
Kita, J. and Ohsumi, T.: Perspectives on Biological Research for CO_2 Ocean Sequestration, J. Oceanogr., 60, 695–703, doi:10.1007/s10872-004-5762-1, 2004. 15789

Koertzinger, A.: Determination of carbon dioxide partial pressure (pCO_2), in: Methods of Seawater Analysis, edited by: Grasshoff, K., Kremling, K., and Erhardt, M., 149–158, Wiley-VCH, Weinheim, 1999. 15792

Marchetti, C.: On geoengineering and the CO_2 problem, Climatic Change, 1, 59–68, doi:10.1007/BF00162777, 1977. 15789

Mayol, E., Ruiz-Halpern, S., Duarte, C. M., Castilla, J. C., and Pelegrí, J. L.: Coupled CO_2 and O_2-driven compromises to marine life in summer along the Chilean sector of the Humboldt Current System, Biogeosciences, 9, 1183–1194, doi:10.5194/bg-9-1183-2012, 2012. 15807

Meehl, G. A., Stocker, T. F., Collins, W. D., Friedlingstein, P., Gaye, A. T., Gregory, J. M., Kitoh, A., Knutti, R., Murphy, J. M., Noda, A., Raper, S. C. B., Watterson, I. G., Weaver, A. J., and Zhao, Z.-C.: Global Climate Projections, in: Climate Change 2007: The Physical Science Basis. Contribution of Working Group I to the Fourth Assessment Report of the Intergovernmental Panel on Climate Change, edited by: Solomon, S., Qin, D., Manning, M., Chen, Z., Marquis, M., Averyt, K. B., Tignor, M., and Miller, H. L., Cambridge University Press, Cambridge, UK and New York, NY, USA, 2007. 15789, 15800

Millero, F. J.: Thermodynamics of the Carbon-Dioxide System in the Oceans, Geochim. Cosmochim. Ac., 59, 661–677, 1995. 15794

Millero, F. J. and Poisson, A.: International One-Atmosphere Equation of State of Seawater, Deep-Sea Res., 28, 625–629, 1981. 15792

Millero, F. J., Graham, T. B., Huang, F., Bustos-Serrano, H., and Pierrot, D.: Dissociation constants of carbonic acid in seawater as a function of salinity and temperature, Mar. Chem., 100, 80–94, 2006. 15800

Orr, J. C., Fabry, V. J., Aumont, O., Bopp, L., Doney, S. C., Feely, R. A., Gnanadesikan, A., Gruber, N., Ishida, A., Joos, F., Key, R. M., Lindsay, K., Maier-Reimer, E., Matear, R., Monfray, P., Mouchet, A., Najjar, R. G., Plattner, G. K., Rodgers, K. B., Sabine, C. L., Sarmiento, J. L., Schlitzer, R., Slater, R. D., Totterdell, I. J., Weirig, M. F., Yamanaka, Y., and Yool, A.: Anthropogenic ocean acidification over the twenty-first century and its impact on calcifying organisms, Nature, 437, 681–686, 2005. 15789

Perry, S. F., Braun, M. H., Genz, J., Vulesevic, B., Taylor, J., Grosell, M., and Gilmour, K. M.: Acid-base regulation in the plainfin midshipman (Porichthys notatus): an aglomerular marine teleost, J. Comp. Physiol. B, 180, 1213–1225, 2010. 15790

Pinczewski, W. V. and Sideman, S.: A model for mass (heat) transfer in turbulent tube flow, Moderate and high Schmidt (Prandtl) numbers, Chem. Eng. Sci., 29, 1969–1976, doi:10.1016/0009-2509(74)85016-5, 1974. 15814

Poertner, H. O., Langenbuch, M., and Michaelidis, B.: Synergistic effects of temperature extremes, hypoxia, and increases in CO_2 on marine animals: From Earth history to global change, J. Geophys. Res.-Oceans, 110, C09S10, doi:10.1029/2004JC002561, 2005. 15797

Royal Society: Ocean Acidification Due to Increasing Atmospheric Carbon Doxide, Policy Document 12/05, The Royal Society, London, UK, 2005. 15789

Sabine, C. L., Feely, R. A., Gruber, N., Key, R. M., Lee, K., Bullister, J. L., Wanninkhof, R., Wong, C. S., Wallace, D. W. R., Tilbrook, B., Millero, F. J., Peng, T. H., Kozyr, A., Ono, T., and Rios, A. F.: The oceanic sink for anthropogenic CO_2, Science, 305, 367–371, 2004. 15790

Santschi, P. H., Anderson, R. F., Fleisher, M. Q., and Bowles, W.: Measurements of Diffusive Sublayer Thicknesses in the Ocean by Alabaster Dissolution, and Their Implications for the Measurements of Benthic Fluxes, J. Geophys. Res., 96, 10641–10657, 1991. 15814

Sarmiento, J. L. and Toggweiler, J. R.: A New Model for the Role of the Oceans in Determining Atmospheric PCO_2, Nature, 308, 621–624, 1984. 15790

Sarmiento, J. L., Le Quéré, C., and Pacala, S. W.: Limiting future atmospheric carbon dioxide, Global Biogeochem. Cy., 9, 121–137, doi:10.1029/94GB01779, 1995. 15790

Seibel, B. A. and Walsh, P. J.: Potential Impacts of CO_2 Injection on Deep-Sea Biota, Science, 294, 319–320, doi:10.1126/science.1065301, 2001. 15790

Seibel, B. A. and Walsh, P. J.: Biological impacts of deep-sea carbon dioxide injection inferred from indices of physiological performance, J. Exp. Biol., 206, 641–650, 2003. 15790, 15807

Shaffer, G., Olsen, S. M., and Pedersen, J. O. P.: Long-term ocean oxygen depletion in response to carbon dioxide emissions from fossil fuels, Nat. Geosc., 2, 105–109, doi:10.1038/NGEO420, 2009. 15789, 15790

Shaw, D. A. and Hanratty, T. J.: Turbulent mass transfer rates to a wall for large Schmidt numbers, AICHE J., 23, 28–37, doi:10.1002/aic.690230106, 1977. 15814

Siegenthaler, U. and Wenk, T.: Rapid Atmospheric CO_2 Variations and Ocean Circulation, Nature, 308, 624–626, 1984. 15790

Soetaert, K., Petzoldt, T., and Meysman, F.: marelac: Tools for Aquatic Sciences, available at: http://CRAN.R-project.org/package=marelac, r package version 2.1, 2010. 15814

Sternberg, R. W.: Friction factors in tidal channels with differing bed roughness, Mar. Geol., 6, 243–260, doi:10.1016/0025-3227(68)90033-9, 1968. 15814

Wanninkhof, R.: Relationship between Wind-Speed and Gas-Exchange over the Ocean, J. Geophys. Res.-Oceans, 97, 7373–7382, 1992. 15814
Weiss, R. F.: Carbon dioxide in water and seawater: the solubility of a non-ideal gas, Mar. Chem., 2, 203–215, 1974. 15792
Wood, P. E. and Petty, C. A.: New model for turbulent mass transfer near a rigid interface, AICHE J., 29, 164–167, doi:10.1002/aic.690290126, 1983. 15814
Zeebe, R. E. and Wolf-Gladrow, D.: CO_2 in Seawater: Equilibrium, Kinetics, Isotopes, no. 65 in: Elsevier Oceanography Series, Elsevier, first edn., 2001. 15792, 15793, 15794, 15795
Zeebe, R. E., Zachos, J. C., Caldeira, K., and Tyrrell, T.: Oceans – Carbon emissions and acidification, Science, 321, 51–52, 2008. 15789, 15800

Table 1. Expressing the DBL thickness L as a function of water flow velocity: a generic planar surface description.

The DBL thickness for CO_2 L^{CO_2} can be expressed as the fraction of the temperature-dependent molecular diffusion coefficient D^{CO_2} for CO_2 in $cm^2\,s^{-1}$, calculated from temperature and salinity as given in Boudreau (1996, Chapter 4) using the implementation in the R package marelac (Soetaert et al., 2010), and the mass transfer coefficient K_{CO_2} (Santschi et al., 1991; Boudreau, 1996)

$$L^{CO_2} = \frac{D^{CO_2}}{K_{CO_2}} \tag{22}$$

K_{CO_2} can be calculated for CO_2 from the water-flow induced shear velocity u' in $cm\,s^{-1}$ and the dimensionless Schmidt number Sc for CO_2 (as calculated by linearly interpolating two temperature dependent formulations for $S = 35$ and $S = 0$ in Wanninkhof (1992) with respect to given salinity)

$$K_{CO_2} = a\,u'\,Sc_{CO_2}^{-b} \tag{23}$$

with parameters a and b: Santschi et al. (1991): $a = 0.078$, $b = \frac{2}{3}$; Shaw and Hanratty (1977) (also given in Boudreau, 1996): $a = 0.0889$, $b = 0.704$; Pinczewski and Sideman (1974) as given in Boudreau (1996): $a = 0.0671$, $b = \frac{2}{3}$; Wood and Petty (1983) as given in Boudreau (1996): $a = 0.0967$, $b = \frac{7}{10}$. Due to small differences we use averaged results of all formulations.

u' can be calculated from the ambient current velocity at 100 cm away from the exchange surface u_{100} and the dimensionless drag coefficient c_{100} (Sternberg, 1968; Santschi et al., 1991; Biron et al., 2004)

$$u' = u_{100}\,\sqrt{c_{100}} \tag{24}$$

c_{100} is calculated from the water flow velocity u_{100} as (Hickey et al., 1986; Santschi et al., 1991)

$$c_{100} = 10^{-3}\,\left(2.33 - 0.0526\,|u_{100}| + 0.000365\,|u_{100}|^2\right) \tag{25}$$

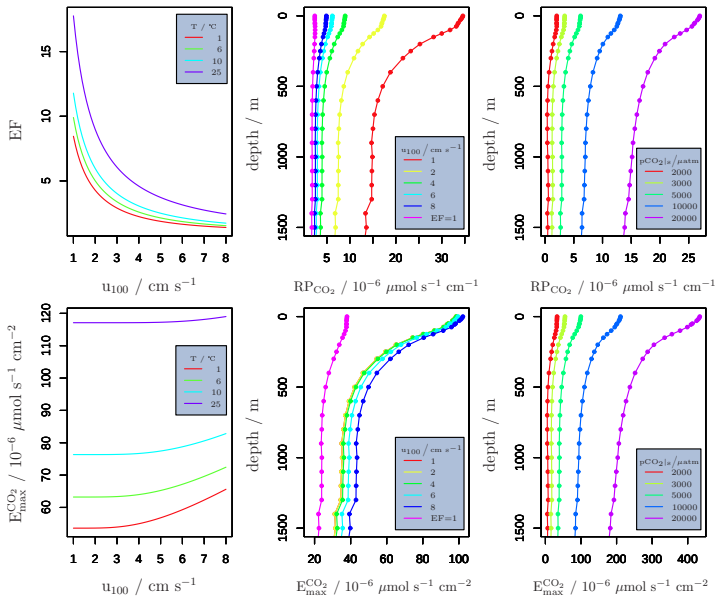

Fig. 1. Sensitivity of derived quantities RP_{CO_2} (the oceanic CO_2 removal potential) and $E_{max}^{CO_2}$ (the maximal CO_2 diffusion limited metabolic rate) with respect to the free stream fluid flow velocity u_{100} and the maximal CO_2 partial pressure in molecular contact with the organism surface ($(pCO_2|_s =) \, pCO_2|_s^{max}$). Left panel, upper row: the enhancement factor EF as a function of the free stream fluid flow velocity u_{100} and temperature T. $[\sum CO_2] = 1900\,\mu mol\,kg^{-1}$, $[TA] = 2050\,\mu mol\,kg^{-1}$, $S = 34$, depth = 100 m, latitude = 30°. Central panel, upper row: example depth profiles at the Southern California (SC: 120.5° W, 29.50° N) station (data from Goyet et al., 2000) of RP_{CO_2}, calculated with varying free stream fluid flow velocities u_{100} and assuming EF = 1. $pCO_2|_s^{max} = 5000\,\mu atm$. Right panel, upper row: example depth profiles at the Southern California (SC) station of RP_{CO_2}, calculated with varying values for the CO_2 partial pressure in molecular contact with the organism surface ($pCO_2|_s =) \, pCO_2|_s^{max}$. $u_{100} = 6\,cm\,s^{-1}$. Left panel, bottom row: $E_{max}^{CO_2}$ as a function of the free stream fluid flow velocity u_{100} and temperature T. $[\sum CO_2] = 1900\,\mu mol\,kg^{-1}$, $[TA] = 2050\,\mu mol\,kg^{-1}$, $S = 34$, depth = 100 m, latitude = 30 °, $pCO_2|_s^{max} = 5000\,\mu atm$. Central panel, bottom row: example depth profiles at the Southern California (SC) station of $E_{max}^{CO_2}$, calculated with varying free stream fluid flow velocities u_{100} and assuming EF = 1. $pCO_2|_s^{max} = 5000\,\mu atm$. $u_{100} = 6\,cm\,s^{-1}$ for the calculation of L^{CO_2} in the EF = 1 case. Right panel, bottom row: Example depth profiles at the Southern California (SC) station of $E_{max}^{CO_2}$, calculated with varying values for the CO_2 partial pressure in molecular contact with the organism surface ($pCO_2|_s =) \, pCO_2|_s^{max}$. $u_{100} = 6\,cm\,s^{-1}$.

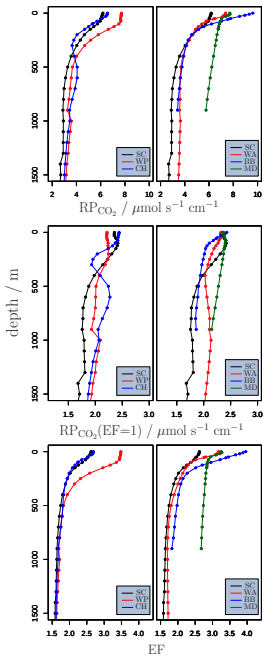

Fig. 2. Example depth profiles of the derived diffusive CO_2 export limitation quantity RP_{CO_2} (the oceanic CO_2 removal potential). Top row: RP_{CO_2} calculated using the chemical enhancement factor EF according to Eq. (9) with $u_{100} = 6\,cm\,s^{-}1$. Central row: RP_{CO_2} calculated assuming no chemical enhancement (i.e., EF = 1). Bottom row: EF calculated according to Eq. (9) with $u_{100} = 6\,cm\,s^{-}1$. $pCO_2|_s^{max} = 5000\,\mu atm$. Oceanographical data are taken from Goyet et al. (2000) and limited to shallower depths when discontinuities occurred deeper (SC: Southern California (120.5° W, 29.50° N); CH: Chile (75.5° W, 33.5° S); WP: Western Pacific (126.5° E, 11.5° N), WA: Western Africa (6.5° E, 15.5° S), MD: Mediterranean (18.5° E, 35.5° N); BB: Bay of Bengal (87.5° E, 18.5° N)).

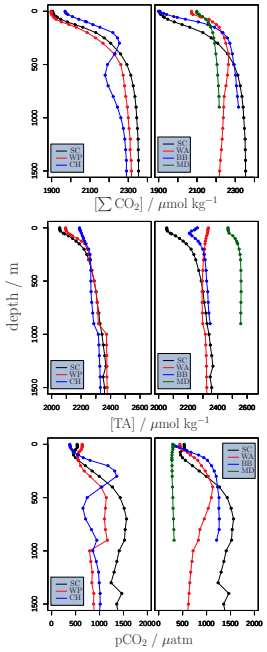

Fig. 3. Oceanographical data taken from Goyet et al. (2000) and limited to shallower depths when discontinuities occurred deeper. Top row: total dissolved inorganic carbon concentration [$\sum CO_2$]. Central row: total alkalinity concentration [TA]. Bottom row: carbon dioxide partial pressure pCO_2. (SC: Southern California (120.5° W, 29.50° N); CH: Chile (75.5° W, 33.5° S); WP: Western Pacific (126.5° E, 11.5° N), WA: Western Africa (6.5° E, 15.5° S), MD: Mediterranean (18.5° E, 35.5° N); BB: Bay of Bengal (87.5° E, 18.5° N)).

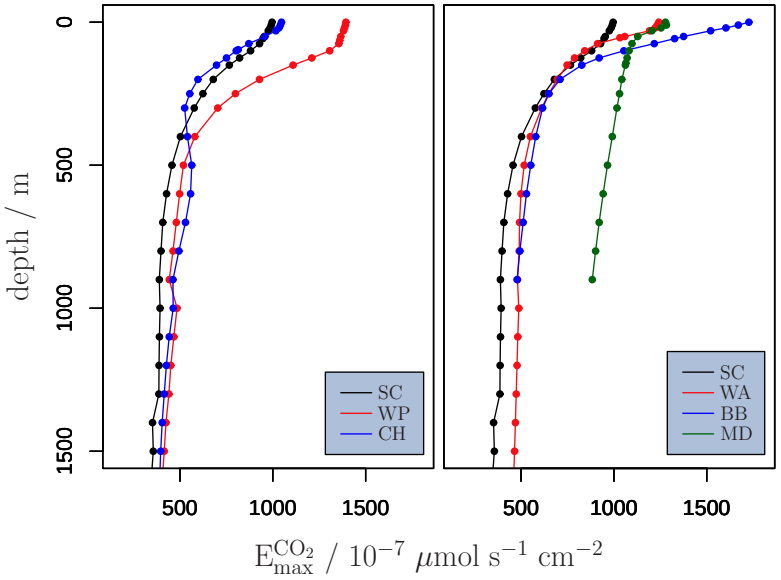

Fig. 4. Example depth profiles of the derived diffusive CO_2 export limitation quantity $E_{max}^{CO_2}$ (the maximal CO_2 diffusion limited metabolic rate). $pCO_2|_s^{max} = 5000\,\mu atm$. Oceanographical data are taken from Goyet et al. (2000) and limited to shallower depths when discontinuities occurred deeper (SC: Southern California (120.5° W, 29.50° N); CH: Chile (75.5° W, 33.5° S); WP: Western Pacific (126.5° E, 11.5° N), WA: Western Africa (6.5° E, 15.5° S), MD: Mediterranean (18.5° E, 35.5° N); BB: Bay of Bengal (87.5° E, 18.5° N)).

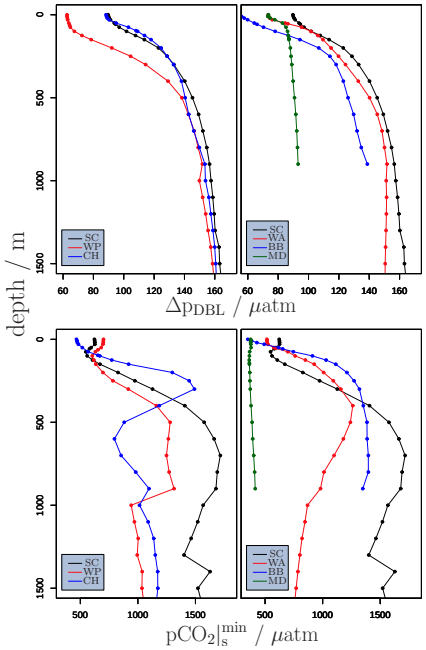

Fig. 5. Example depth profiles of the derived diffusive CO_2 export limitation quantities based on a given metabolic rate $E^{O_2} = 20 \times 10^{-7}$ µmol s^{-1} cm^{-2}. Top panel: Δp_{DBL} (the minimal CO_2 partial pressure differential across the DBL required to sustain a given metabolic rate). Bottom panel: $pCO_2|_s^{min}$ (the minimal CO_2 partial pressure in molecular contact with a gas exchange surface that sustains a given metabolic rate under given external oceanic conditions). Oceanographical data are taken from Goyet et al. (2000) and limited to shallower depths when discontinuities occurred deeper (SC: Southern California (120.5° W, 29.50° N); CH: Chile (75.5° W, 33.5° S); WP: Western Pacific (126.5° E, 11.5° N), WA: Western Africa (6.5° E, 15.5° S), MD: Mediterranean (18.5° E, 35.5° N); BB: Bay of Bengal (87.5° E, 18.5° N)).

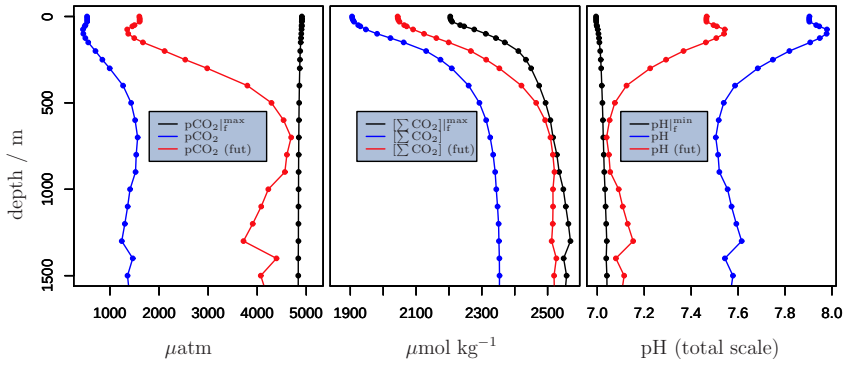

Fig. 6. Example depth profiles for the Southern California example station (SC, 120.5° W, 29.50° N) of limiting external conditions calculated based on derived diffusive CO_2 export limitation quantities assuming a given metabolic rate $E^{O_2} = 20 \times 10^{-7}$ µmol s^{-1} cm^{-2} and a given maximal pCO_2 in molecular contact with the gas exchange surface $pCO_2|_s^{max}$ = 5000 µatm. Left panel: $pCO_2|_f^{max}$ (the maximal CO_2 partial pressure in the external bulk free stream that sustains a given metabolic rate; black line), compared to present-day ambient pCO_2 values (blue line) and assumed "future" pCO_2 values (red line, a tripled pCO_2 in the whole water column). Center panel: $[\sum CO_2]|_f^{max}$ (the maximal dissolved inorganic carbon concentration, as calculated from $pCO_2|_f^{max}$, sustaining a given metabolic rate; black line) compared to present-day $[\sum CO_2]$ values (blue line) and assumed "future" $[\sum CO_2]$ values (red line; consistent with a tripled pCO_2 in the whole water column). Right panel: $pH|_f^{min}$ (the minimal external total scale pH, as calculated from $pCO_2|_f^{max}$, sustaining a given metabolic rate; black line), compared to present-day total scale pH values (blue line), and assumed 'future" pH values (red line; consistent with a tripled pCO_2 in the whole water column). Oceanographical data are taken from Goyet et al. (2000).

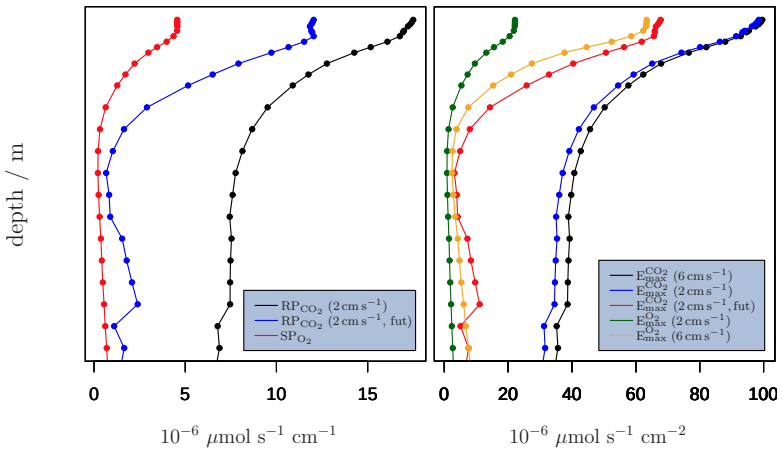

Fig. 7. Example depth profiles for the Southern California example station (SC, 120.5° W, 29.50° N) of diffusive carbon dixoide export limitation quantities as defined here, compared to equivalent diffusive oxygen uptake limitation quantities defined in the companion paper Hofmann et al. (2012). Left panel: RP_{CO_2} (the oceanic CO_2 removal potential) calculated with $u_{100} = 2\,\mathrm{cm\,s^{-1}}$ and current ambient pCO_2 values (black line) and assumed "future" tripled pCO_2 values (blue line), compared to SP_{O_2} (the oceanic oxygen supply potential, calculated according to Hofmann et al., 2012). Right panel: $E^{CO_2}_{max}$ (the maximal CO_2 diffusion limited metabolic rate), calculated with various given values for the fluid flow velocity u_{100}, and current and future pCO_2 conditions, compared to $E^{O_2}_{max}$ (the maximal O_2 diffusion limited metabolic rate, calculated according to Hofmann et al. (2012) with various u_{100} values and current oxygenation conditions). Oceanographical data for CO_2 are taken from the Goyet et al. (2000) climatology. Oceanographical data for O_2 are taken from the Garcia et al. (2010) oxygen climatology.